Event-by-Event Image Reconstruction From List-Mode PET Data

Colas Schretter

***Abstract*—This paper adapts the classical list-mode OSEM and the globally convergent list-mode COSEM methods to the special case of singleton subsets. The image estimate is incrementally updated for each coincidence event measured by the PET scanner. Events are used as soon as possible to improve the current image estimate, and, therefore, the convergence speed toward the maximum-likelihood solution is accelerated. An alternative online formulation of the list-mode COSEM algorithm is proposed first. This method saves memory resources by re-computing previous incremental image contributions while processing a new pass over the complete dataset. This online expectation-maximization principle is applied to the list-mode OSEM method, as well. Image reconstructions have been performed from a simulated dataset for the NCAT torso phantom and from a clinical dataset. Results of the classical and event-by-event list-mode algorithms are discussed in a systematic and quantitative way.**

***Index Terms*—Event-by-event (EBE), expectation-maximization (EM), list-mode (LM), maximum-likelihood (ML), ordered subsets (OS), positron emission tomography (PET).**

I. INTRODUCTION

STATISTICAL image reconstruction methods from list-mode emission tomography data are more and more popular and the reasons for this success are manifold. These methods estimate the image that best fits the data in terms of Poisson maximum-likelihood (ML) and support implicitly noisy measurements. Furthermore, using a sequential list-mode data model exploits the high-precision spatial and temporal information of emission measures in a natural way. In contrast, histogram data models allow random access to consult the total of measures along any pair of detectors, called line of response (LOR). However, while histograms need to be loaded in memory, a list-mode instance can be streamed from disk storage and processed event-by-event.

An additional motivation for list-mode image reconstructions comes from the fact that the number of detectors of modern positron emission tomography (PET) scanners increases continuously. Since the number of LORs follows a quadratic law with the number of detectors, nowadays, the typical number of events of a list-mode dataset has fallen below the number of possible LORs.

The gold standard of statistical reconstruction makes use of the maximum-likelihood expectation-maximization (MLEM) algorithm which was proposed by Shepp and Vardi in 1982 [1] and adapted to list-mode data by Barrett *et al.* in 1997 [2]. The complete dataset is used to compute a multiplicative correction factor for each image element. The MLEM is a globally convergent algorithm, i.e., it tends to a unique image regardless of the initialization. Unfortunately, many iterations are needed to yield an acceptable reconstruction.

An accelerated version of the MLEM algorithm, the ordered subsets MLEM (OSEM), was proposed by Hudson and Larkin in 1994 [3]. The idea of OSEM is to consider only a subset of the input data to approximate the correction factors. The dataset is split into disjoint subsets, containing a roughly equal number of events. A new image is estimated after each sub-iteration.

The OSEM method is not convergent in the general case. Nevertheless, OSEM became a standard for clinical applications, due to its good experimental trade-off between speed and quality, making possible statistical reconstructions from realistic datasets with shorter reconstruction times than acquisition duration. In 2000, the adaptation of OSEM to list-mode data by Reader *et al.* [4], [5] has demonstrated impressive results in terms of image quality and reconstruction speed.

In 2002, Hsiao *et al.* [6] proposed an elegant globally convergent ordered subsets method, the complete-data OSEM (COSEM), that has been adapted to list-mode by Khurd *et al.* in 2004 [7]. This algorithm not only makes use of events in the current subset for estimating the image, but also takes into account contributions from previous image estimates that depend on the other subsets. Note that the COSEM method of Levkovitz *et al.* [8] is related to a list-mode extension of OSEM and has no relation with the algorithm considered here.

The COSEM method is very attractive but raises some questions. The convergence is slower than using OSEM (assuming that OSEM converges for the given dataset) and the number of subsets must be specified by the user, as for OSEM. The more subsets you use, the faster the algorithm converges. However, since the algorithm needs to remember the previous intermediate results for each image element and for each subset, a large amount of memory room is often required for high-resolution 3-D image reconstruction.

The convergence speed of the COSEM method has been improved recently, in 2004 [9] with the enhanced COSEM (ECOSEM) algorithm. The approach suggests to perform two estimations in parallel: the first, using OSEM and the second, using COSEM. The image is updated with a linear combination of these two estimates to trade speed with stability. Since the first term of the ECOSEM sum is exactly equivalent to the OSEM estimate for the current subset, no additional computation for this term is needed. Independently and simultaneously, this hybrid approach has been applied for list-mode data by

Manuscript received December 25, 2006; revised May 21, 2008. The associate editor coordinating the review of this manuscript and approving it for publication was Prof. Peter C. Doerschuk.

The author is with the TEP/Cyclotron Biomédical Unit, Erasme hospital, Université libre de Bruxelles (ULB), Brussels, Belgium (e-mail: cschrett@ulb.ac.be).

Digital Object Identifier 10.1109/TIP.2008.2007756

Rahmim *et al.* [10]. The authors simply suggest to use OSEM for early sub-iterations, then switching to COSEM for polishing the image.

The present work proposes two algorithms for updating the emission image as soon as an event is read from the list-mode dataset. These event-by-event reconstruction methods correspond to an online EM algorithm as proposed in the paper of Neal and Hinton [11]. This approach also follows the spirit of the row-action maximum-likelihood algorithm (RAMLA) [12] that updates the current image for each projection of an histogram. However, each image update does not need to be weighted by a relaxation parameter and the globally convergent event-by-event reconstruction method does not require specifying a number of subsets.

After defining the notations in Section II, two event-by-event algorithms are presented in Section III. The first algorithm (EBE-COSEM) is proven to be globally convergent. The second algorithm (EBE-OSEM) is not convergent but produces a sharp image much faster. The results are discussed in Section IV and confirm the theoretical improvement of convergence speed towards the maximum-likelihood solution for both methods. Finally, conclusions and tracks for future work are proposed in Section V.

II. Notations for List-Mode Algorithms

All statistical list-mode algorithms estimate a set M of image bins from a list N of events. The complete data N can be partitioned into L disjoint subsets

$$N = \biguplus_{l=0}^{L-1} S_l \tag{1}$$

with $0 \leq l < L$ and $1 \leq L \leq |N|$. The subsets $S_l \subset N$ contain roughly the same number of events.

Iterative list-mode image reconstruction methods will be defined by relating the successive values of each image bin. The intermediate formula

$$\tilde{\lambda}_j^{n+1} = \frac{\lambda_j^n}{w_j} \sum_{i \in S_l} \frac{A_{ij}}{a_i \sum\limits_{k \in M} A_{ik} \lambda_k^n}, \quad l = \left\lfloor \frac{n \bmod |N|}{L} \right\rfloor \tag{2}$$

will be used as a building block for the definition of list-mode algorithms in a unified notation.

λ_j^{n+1} is the current value of image bin $j \in M$ after processing $n+1$ events. For the algorithms that will be defined in (6), (7), and (10), the estimation starts from a uniform image $\lambda_j^0 = 1$, $\forall\, j \in M$. The initial images of previous steps are assumed to be empty; hence, $\lambda_j^{-s} = 0, \forall\, j \in M, s \geq 1$.

A_{ij} is equal to the probability that an annihilation occurring in image bin $j \in M$ is detected along the LOR of the event $i \in N$. The system matrix A is very large and often sparse. Hence, its elements are usually computed on-the-fly by ray-tracing techniques [13] to avoid storage of the matrix in memory.

Sometimes, the probability A_{ij} is assumed to be proportional to the length of intersection of the LOR of the event $i \in N$ with the image bin $j \in M$. If bins are pixels or voxels, such an intersection computation is fast and straightforward [14]. Instead, this work relies on a refined ray-tracer [15] that models volumetric tubes of responses to account for the finite spatial resolution of voxel grids.

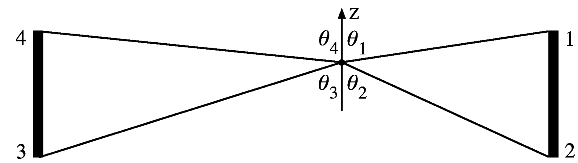

Fig. 1. Four angles considered for integration of the sensitivity factor at a given position. In this case, the two maximum angles are θ_3 and θ_4. The larger the angles, the lower the cosine of the angles, hence the sensitivity.

w_j are sensitivity factors, equal to the probability that an annihilation occurring in image bin $j \in M$ is detected by the PET scanner. These factors are proportional to the solid-angle that the detector edge subtends at the center of the voxels and are defined by

$$w_j = \int_0^{\pi/2} \cos\left(\max\{\theta_1, \theta_3\}\right) + \cos\left(\max\{\theta_2, \theta_4\}\right)\, d\phi \tag{3}$$

where $\{\theta_1, \theta_2, \theta_3, \theta_4\}$ are the angles between the depth axis and the vectors joining the center of the voxel to each of the four clockwise-ordered vertices of the intersection between the detector cylinder and the coronal plane of angle ϕ, passing through the center of the given voxel $j \in M$.

In (3), the two maximum angles of nondetection are considered since both collinear photons must hit the cylinder to produce an event. An illustration is given in Fig. 1. Note that for any point (x, y, z) in the field of view, the sensitivity only depends on the distance to the depth axis $\sqrt{x^2 + y^2}$ and the z coordinate of this point. In this work, the continuous integral is approximated[1] by numerical integration, using a fixed step of one degree.

a_i are attenuation factors [16], equal to the probability that the two collinear photons are not absorbed during their flight along the LOR of the event $i \in N$ whose length in centimeter equals l_i. According to Beer's law, this probability can be approximated by

$$a_i = \exp\left(-l_i \sum_{k \in M} A_{ik} \mu_k\right) \tag{4}$$

where μ_j, $\forall\, j \in M$ is an attenuation image containing linear factors for each voxel.

Attenuation factors are calculated for each event by ray-tracing along its LOR. In experiments, the attenuation image is derived by segmentation of a registered anatomical image in three different materials (air, lungs, organs). The conventional factors (0, 0.035/cm, 0.095/cm) for photons at 511-keV energy are used to map every voxel $j \in M$ on its corresponding linear attenuation factor μ_j, in function of the label of his material.

[1]The sensitivity factors can also be approximated by running a Monte-Carlo simulation of the emission process with a nonattenuating uniform cylinder that fill the field of view of the scanner. However, the computing time is much larger and even with an extremely large number of samples, the sensitivity information is difficult to resolve at the axial extremities of the detector.

A. LM-EM, LM-OSEM, LM-COSEM, and LM-ECOSEM

When more than one subset $(L > 1)$ is used, the LM-OSEM algorithm replaces the current image estimate with a new estimate, computed only from the events of the next subset. Using the intermediate result in (2) yields the following notation:

$$\lambda_j^{n+1} = L\tilde{\lambda}_j^{n+1}. \tag{5}$$

LM-OSEM considers only a subset $S_l \subset N$ of the input data to evaluate the multiplicative correction factor for each image bin. A new image is estimated after each sub-iteration and a full iteration is over when every event of the list-mode file has been processed. LM-EM is a special case of LM-OSEM with only one subset $(L = 1)$, hence $S_0 = N$. On the other hand, the LM-COSEM algorithm sums up the intermediate results to ensure global convergence and can be denoted by

$$\lambda_j^{n+1} = \sum_{s=0}^{L-1} \tilde{\lambda}_j^{n+1-s}. \tag{6}$$

In LM-COSEM, a new term enters the sum to replace the previous image contributions corresponding to the current subset. The following incremental update is equivalent to (6)

$$\lambda_j^{n+1} = \lambda_j^n + \tilde{\lambda}_j^{n+1} - \tilde{\lambda}_j^{n+1-L}. \tag{7}$$

The linear combination of (5) and (7) yields the LM-ECOSEM algorithm denoted by

$$\lambda_j^{n+1} = t(n)\, L\tilde{\lambda}_j^{n+1} + (1 - t(n)) \left(\lambda_j^n + \tilde{\lambda}_j^{n+1} - \tilde{\lambda}_j^{n+1-L}\right) \tag{8}$$

where $t(n)$ with $0 \leq t(n) \leq 1$, is a trade-off parameter that balances speed and convergence.

III. Event-by-Event Expectation-Maximization

This section investigates the behavior of LM-COSEM when the number of subsets is equal to the number of detected coincident events. In this case, a subset consists of a single event, and, therefore, the image estimate will be updated every time an event is read from the list-mode dataset. This approach is motivated by the hope to significantly improve convergence speed because it allows direct improvement of the image estimate with additional statistical information, as soon as events are processed.

Because of the similarity with the LM-COSEM method, the event-by-event reconstruction can be theoretically justified by a simplified convergence proof in the optimization transfer framework of Ahn *et al.* [17]. In fact, the proposed algorithm is derived from a special case of LM-COSEM and, thus, benefits from its theoretical properties [7]. In particular, LM-COSEM has been proven to be globally convergent for any number of subsets, hence, for singleton subsets. Furthermore, the convergence speed of EBE-COSEM is theoretically maximized [5] since the maximal number of subsets is used.

Reducing the number of events per subset down to one poses a number of problems because each image update will only affect the voxels located along the LOR of the considered event. In addition, storing one image per subset, as required by LM-COSEM, becomes impractical. Solutions exists to overcome these problems.

A. EBE-COSEM and EBE-OSEM

The event-by-event COSEM (EBE-COSEM) is a particular case of LM-COSEM, when $L = |N|$. Each subset contains only one event; thus, $S_i = \{i\}$ and the intermediate formula (2) can be simplified to

$$\tilde{\lambda}_j^{n+1} = \frac{A_{ij}\lambda_j^n}{w_j a_i \sum\limits_{k\in M} A_{ik}\lambda_k^n}, \quad i = n \bmod |N|. \tag{9}$$

Inserting (9) into (7) yields the EBE-COSEM algorith

$$\lambda_j^{n+1} = \lambda_j^n + \frac{A_{ij}}{w_j a_i}\left[\frac{\lambda_j^n}{\sum\limits_{k\in M} A_{ik}\lambda_k^n} - \frac{\lambda_j^{n-|N|}}{\sum\limits_{k\in M} A_{ik}\lambda_k^{n-|N|}}\right] \tag{10}$$

where $i = n \bmod |N|$.

For each event $i \in N$, each image bin $j \in M$ will be updated as in the case of LM-COSEM with singleton subsets. For the first iteration, the negative term in (10) is equal to zero and since $n - |N| < 0$, then $\lambda_j^{n-|N|} = 0$ if $0 \leq n < |N|$. Therefore, the algorithm can be simplified for the first pass over the dataset, by ignoring the negative term.

Clearly, only image bins along the LOR of the event will be modified. This locality property makes the implementation of an event-by-event reconstruction feasible. By experience, the computational time per event of this method is equal to the traditional subset-based LM-COSEM.

The event-by-event OSEM (EBE-OSEM) also relies on the incremental image update in (9) and is written

$$\lambda_j^{n+1} = \lambda_j^n + \frac{A_{ij}\lambda_j^n}{w_j a_i \sum\limits_{k\in M} A_{ik}\lambda_k^n} - \Delta_j^n, \quad i = n \bmod |N| \tag{11}$$

with

$$\Delta_j^n = \begin{cases} \lambda_j^{n+1-|S_l|}, & \text{if } n+1 \bmod |N| \notin S_l \\ 0, & \text{otherwise} \end{cases}$$

where $l = \lfloor n \bmod |N|/L \rfloor$.

The EBE-OSEM method only keeps the history of the most recent image contributions that belong to the current subset. Therefore, the image estimate of the previous subset is removed after having processed the last event of a subset.

B. Computing Previous Updates

The result of the first pass over the entire dataset is equivalent to summing contributions of each event, in image space. For the remaining iterations, the previous contribution has to be replaced, event-by-event, with the refined estimate. However, the huge memory resource demand of COSEM methods is a remaining issue. Since it is currently impossible to store the previous values of image bins for each event, these results are re-computed online.

The remaining passes start from the result image λ_j^n of the previous iteration and compute in parallel the new contributions $\tilde{\lambda}_j^{n+1}$ and the previous contributions $\tilde{\lambda}_j^{n+1-L}$ for each image

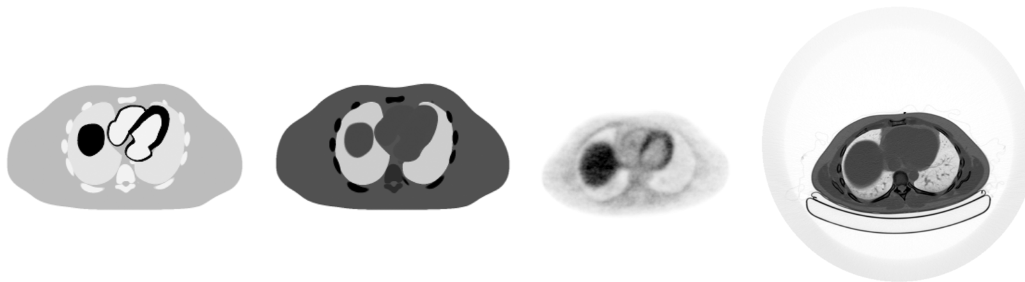

(a) Activity (b) Attenuation (c) ML (d) CT

Fig. 2. Transversal slices of the NCAT phantom and the clinical studies: (a) and (b) are, respectively, the activity and attenuation images of the NCAT phantom; (c) and (d) are, respectively, the maximum-likelihood image of the clinical dataset and the corresponding slice in the CT scan for attenuation.

bin $j \in M$. As shown in (7), the previous estimate of the event in image space is replaced by a refined estimate. An important feature of this approach is that the ray-tracing calculation of any given event $i \in N$, i.e., the computation of the A_{ij}'s for $j \in M$, only needs to be performed once per event.

The new EBE-COSEM formulation defines an online image reconstruction pipeline for list-mode data. The actual implementation provides two routines dedicated respectively to the first and second iteration. A recursive procedure will handle an arbitrary number of passes over the dataset. Of course, the running time of successive iterations increases arithmetically but only two iterations should be sufficient for realistic problem instances [5].

Since re-computation balances the overhead of storing previous estimates, the total reconstruction time of EBE-COSEM is, by experience, equivalent to the time taken by the LM-COSEM method. Therefore, with EBE-COSEM, the COSEM algorithm becomes faster and more applicable for 3-D reconstruction of high resolution images without demanding excessive memory resources.

C. Image Initialization

Any iterative statistical expectation-maximization method needs an initial estimation to start the iterative refinement towards the maximum-likelihood solution. Often, a constant initial image is used, for example $\lambda_j^0 = 1, \forall\, j \in M$. With the event-by-event approach this initial value of image bins can be embedded in the image update operator. Indeed, by starting from an empty image $\lambda_j^0 = 0, \forall\, j \in M$, only the image bins crossed by observed LORs need to be initialized.

Accounting an initialization constant to image bins in (9) yields

$$\tilde{\lambda}_j^{n+1} = \frac{A_{ij}\left(\lambda_j^n\,(1-\varepsilon)+\varepsilon\right)}{w_j a_i \sum\limits_{k\in M} A_{ik}\left(\lambda_k^n\,(1-\varepsilon)+\varepsilon\right)}, \quad i = n \bmod |N| \tag{12}$$

where the additional constant, $0 \leq \varepsilon \leq 1$, can be interpreted as an exploration-exploitation parameter that drives the relative contribution of the current image bin. The exploration-exploitation trade-off is well known in the literature about online learning [18, Ch. 13].

If $\varepsilon = 0$ (full exploitation) then (12) becomes equivalent to (9). On the other hand, if $\varepsilon = 1$ (full exploration) then the relative contribution of image bins vanishes, and (12) becomes equivalent to the backprojection operator that maps an event from data space to bins in image space. The backprojection spreads uniformly the contribution of an event to image elements straddling its LOR.

The parameter ε is set to one during the processing of the first events and then is set to zero for the remaining events. The number of these first events is chosen empirically and is often equal to a typical subset's size. The initial image is then equivalent to the backprojection of these events. So, this processing only initializes image bins crossed by the first events.

IV. Results

Image reconstructions have been performed from a simulated list-mode dataset for the NCAT phantom [19] and from a clinical acquisition of a similar region of the body. The original (LM-OSEM and LM-COSEM) algorithms and their event-by-event variants (EBE-OSEM and EBE-COSEM) are considered for systematic comparisons. The data has been split into eight subsets.

The clinical dataset has been acquired on a Philips Gemini PET/CT scanner with a detector diameter of 86.4 cm, a field of view of 57.6 cm and an axial length of 18.2 cm. A similar detector geometry is modeled for the simulation. The definition of reconstructed images is 295 $\times$ 295 for each of the 92 slices. Image elements are cubic voxels of 2-mm size.

For the NCAT phantom study, a list-mode file of 8 million events has been generated by randomly simulating the emission process from the static emission and attenuation images shown in Fig. 2(a) and (b). About 834 million of samples have been simulated by the Monte-Carlo process. About 752 million events have been attenuated and among the remaining, about 74 million events have been rejected because at least one of the two coincident photons did not hit the cylindrical detector.

For the clinical study, the last time frame of a dynamic $N-13$ (ammonia) cardiac study has been reconstructed. The acquisition began 10 minutes after injection and lasted for 6 min. 370 MBq has been injected for a male of 83 kg. About 84 million coincidences events have been recorded, including delayed events for compensation of randoms. About 24 million events did not cross the prior anatomy image and have been discarded because they are obviously scatters or randoms. The remaining random noise have been corrected according to the advices of Rahmim *et*

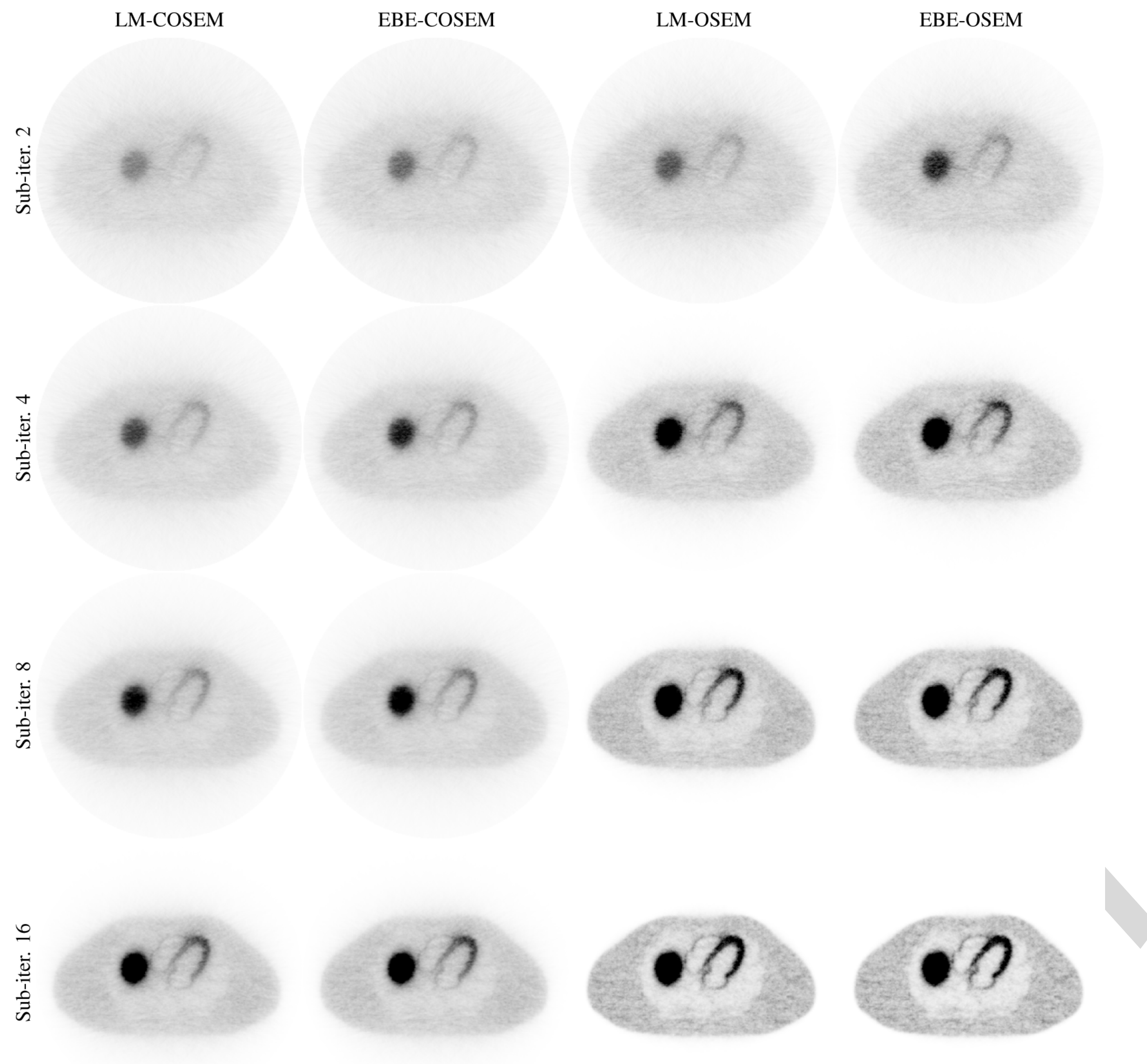

Fig. 3. Transversal slices of reconstructions for the NCAT phantom study. Each row contains the current estimate for the given sub-iteration number. The last row shows the results after two iterations over the data.

al. [10], by subtraction of delayed events while ensuring image non-negativity.

Images are shown in Figs. 3 and 4. The transversal slices 57 have been chosen because they emphasize both the myocardium and the liver. Even for low-statistics estimations of early sub-iterations, the event-by-event reconstructions of the second and fourth columns produce sharper images compared to the results of classical reconstruction methods of the first and third columns.

Graphs are shown in Fig. 5. The volumetric activity image of Fig. 2(a) is considered as reference for the NCAT phantom study and the maximum-likelihood image of Fig. 2(c), reconstructed after 64 iterations of the MLEM algorithm is considered as reference for the clinical study.

Quantitative analysis of the reconstructed images is shown in terms of contrast recovery over variance in the liver and the ventricle, and in terms of Kullback–Leibler (KL) divergence from the reference image. The motivation to use the KL metric over the classical mean square error (MSE) metric is discussed in appendix.

Incremental event-by-event algorithms exhibit similar behaviors, like classical multiplicative algorithms. The contrast recovery is faster; however, the variance inside regions of interest also increases with the fitting of the data. The OSEM methods reach a limit cycle toward the end of the second iteration for both studies. The KL divergence plots show that both classical list-mode and event-by-event list-mode algorithms converge to a similar objective image. The COSEM methods are, however, much slower.

There is no bias in the KL divergence curve of the clinical study because the reference ML image is the result of a reconstruction sharing exactly the same system model than the four compared methods. A sudden hop can be noticed on the curves of the COSEM methods, after the first full iteration over the data. This is due to the subtraction of the very first backprojection image estimate that tends to be very blurred and far from the maximum-likelihood.

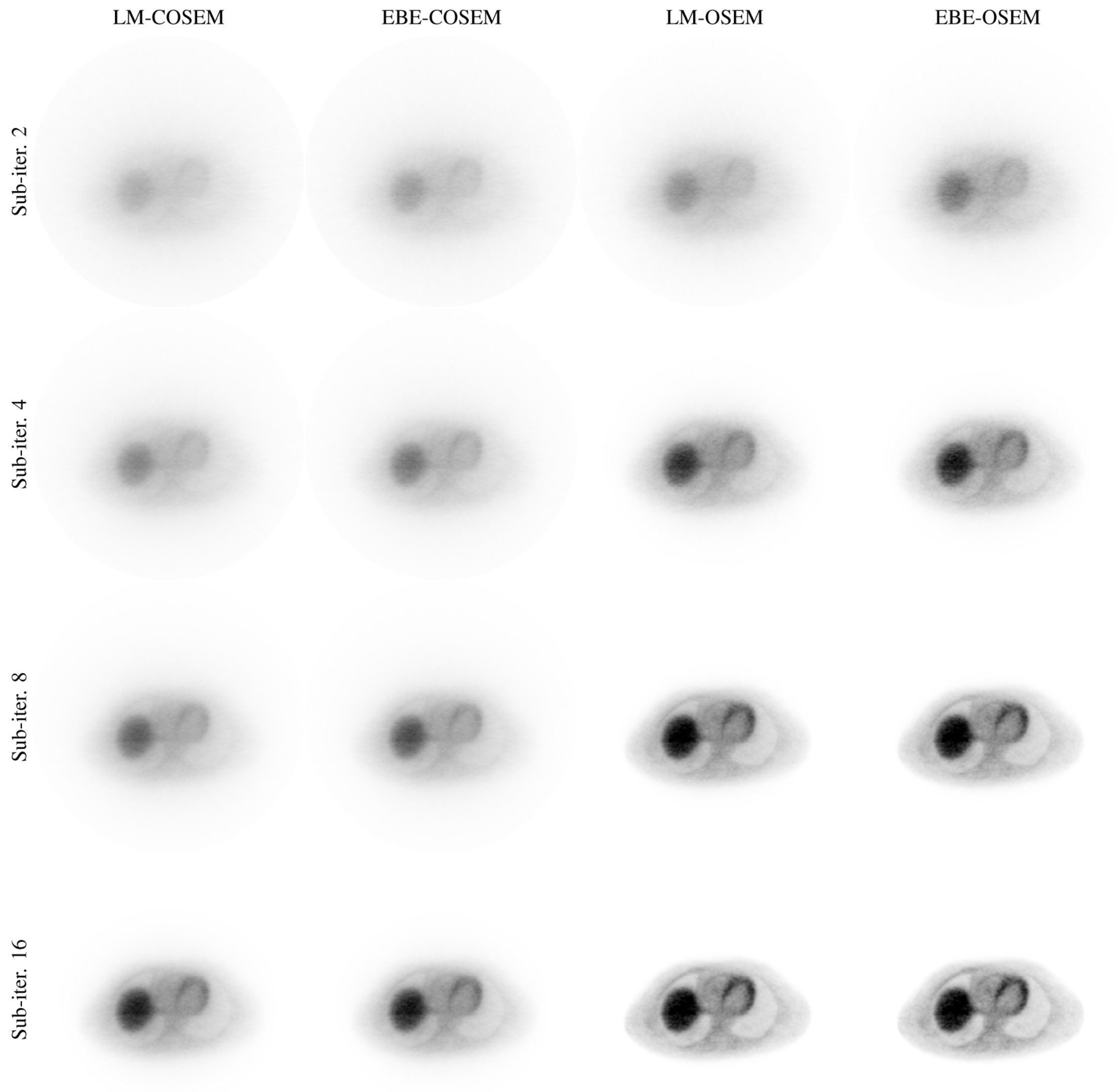

Fig. 4. Transversal slices of reconstructions for the clinical study. Each row contains the current estimate for the given sub-iteration number. The last row shows the results after two iterations over the data.

It is also interesting that, from identical initial conditions, LM-OSEM and EBE-OSEM reach nearly the same point in the graph of contrast recovery over variance in the ventricle: after nine sub-iterations of LM-OSEM but only six sub-iterations of EBE-OSEM.

V. Conclusion

This work aims to show that incrementally updating the current reconstructed image estimate, for each event of list-mode data instances, can improve the convergence speed towards the unknown emission image. The proposed event-by-event reconstruction algorithms directly take into account the statistical contribution of each event to improve the image estimate. These methods converge faster to the maximum-likelihood solution.

An additional feature of the approach is that the number of updates, for each image element, is driven by the number of events passing through it. The likelihood of images produced by iterative algorithms monotonically increases with the number of image updates. Hence, in event-by-event methods, the convergence speed to the maximum-likelihood solution is adapted to the amount of statistical information associated with each image element.

Future work plans to combine the two event-by-event OSEM and COSEM methods in the definition of an hybrid algorithm that could balance speed and convergence, in the spirit of ECOSEM.

Appendix
Comparing Images

Mean Square Error: Often, metrics defined from the mean square error (MSE) are used to evaluate the similarity between two images. However, the MSE metric can be nonappropriate for some quantitative analyses in emission tomography.

Consider a reference image P (ground truth image) and a second image Q (reconstructed image). If both images contain N image elements, the MSE measure of the error between P and Q is

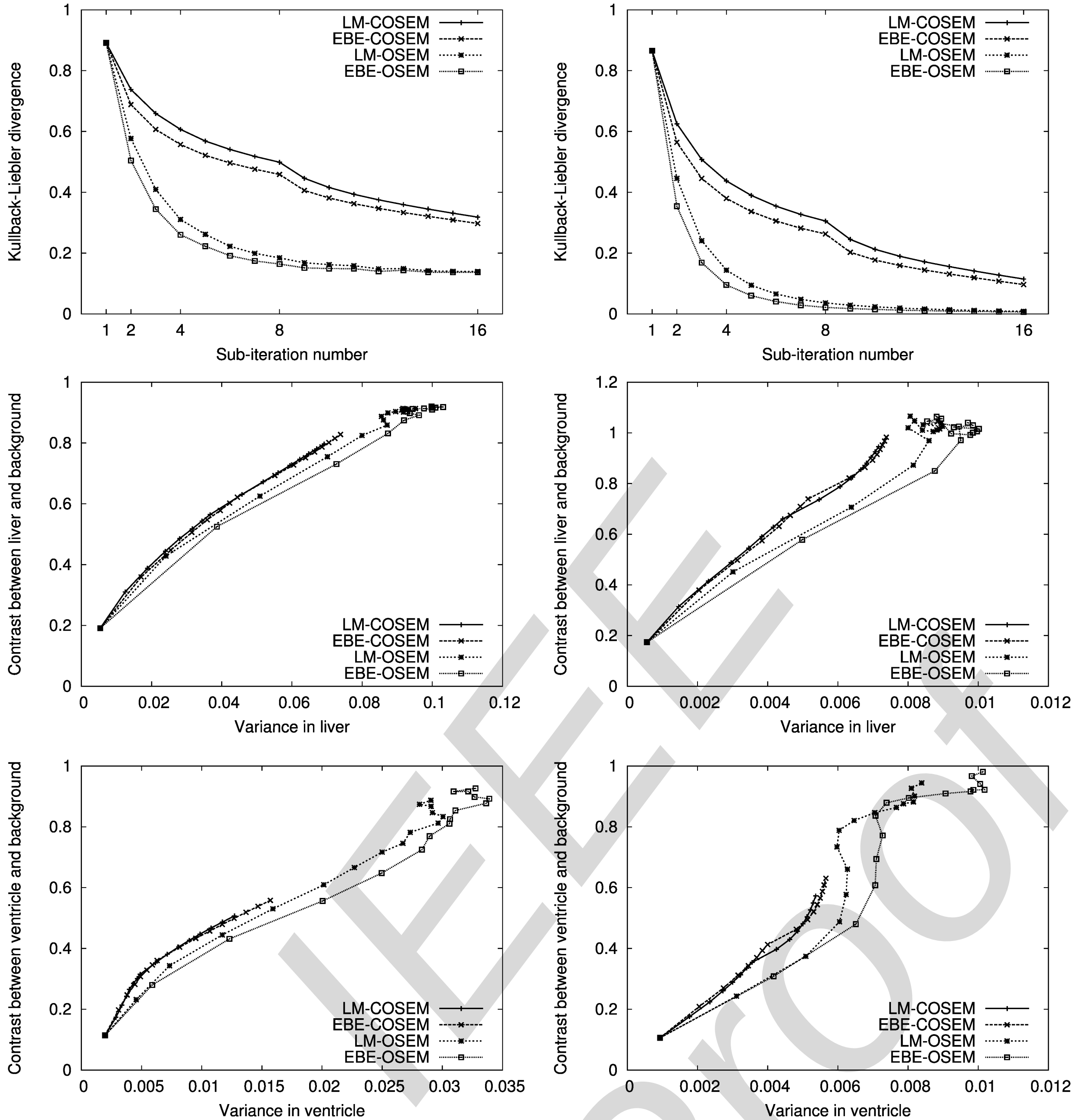

(a) NCAT phantom study

(b) Clinical study

Fig. 5. Figures of quantitative analyses for the NCAT phantom study (a) and the clinical study (b). The three rows show respectively the Kullback–Leibler divergence from the reference activity image and the contrast recovery over variance in the liver, and in the left ventricle.

$$\mathrm{MSE}\,(P,Q) = \frac{1}{N}\sum_{k=1}^{N}(P_k - Q_k)^2.$$

Since the differences between corresponding image elements $(P_k - Q_k)$ are squared, the total MSE is never negative. Furthermore, if $P = Q$, then the MSE is equal to zero. However, large values receive more importance with this metric and the contributions of relative errors between small values vanish. For example, if $P_k = 10$ and $Q_k = 1$, then $(P_k - Q_k)^2 = 9^2 = 81$; but, if $P_k = 100$ and $Q_k = 10$, then $(P_k - Q_k)^2 = 90^2 = 8100$. When evaluating a reconstructed emission image, errors in low-count regions that are badly reconstructed will be ignored if high-count regions are a little bit more accurate.

Relative Entropy: The relative entropy, also known as the Kullback–Leibler (KL) divergence, is used in statistics to compare the similarity between discrete probability density functions (DPDF). This metric could be appropriate to measure the similarity between two images in emission tomography.

Images can be normalized by computing the total sum of image elements and then dividing each image element by this total sum. After normalization, the total sum equals one, and, thus, the images meet the definition of DPDF. Each image element contains the probability that an emission occurs in a part of space (usually square of cubic shaped). Consider P and Q as two DPDFs with N histogram bins. The relative entropy of P with respect to Q is

$$KL(P,Q) = \sum_{k=1}^{N} P_k \log\left(\frac{P_k}{Q_k}\right).$$

Note that this measure is not symmetric because $KL(P,Q) \neq KL(Q,P)$. However, the formula is a convex function of P, is always non-negative, and equals zero only if $P = Q$. Let consider a base two logarithm function, then the relative entropy gives the number of bits that is needed to store Q when the reference image P is known. This metric is appropriate for comparing emission images since statistical reconstructions are in fact estimations of a density function.

ACKNOWLEDGMENT

The author would like to thank Prof. M. Defrise for insightful discussions and J. Mannheim for her help on geometrical sensitivity. He would also like to thank Dr. G. Van Simaeys and Prof. S. Goldman for their medical insights.

REFERENCES

[1] L. A. Shepp and Y. Vardi, "Maximum likelihood reconstruction for emission tomography," *IEEE Trans. Med. Imag.*, vol. MI-4, no. 2, pp. 113–122, Feb. 1982.

[2] H. Barrett, T. White, and L. Parra, "List-mode likelihood," *J. Opt. Soc. Amer. A*, vol. 14, no. 11, pp. 2914–2923, 1997.

[3] H. M. Hudson and R. S. Larkin, "Accelerated image reconstruction using ordered subsets of projection data," *IEEE Trans. Med. Imag.*, vol. 13, no. 4, pp. 601–609, Apr. 1994.

[4] A. J. Reader, S. Ally, F. Bakatselos, R. Manavaki, R. J. Walledge, A. P. Jeavons, P. J. Julyan, S. Zhao, D. L. Hasting, and J. Zweit, "One-pass list-mode EM algorithm for high resolution 3D PET image reconstruction into large arrays," *IEEE Trans. Nucl. Sci.*, vol. 49, no. 3, pp. 693–699, Mar. 2002.

[5] A. Reader, R. Manavaki, S. Zhao, P. Julyan, D. Hasting, and J. Zweit, "Accelerated list-mode EM algorithm," *IEEE Trans. Nucl. Sci.*, vol. 49, no. 1, pp. 42–49, Jan. 2002.

[6] I.-T. Hsiao, A. Rangarajan, and G. Gindi, "A provably convergent OS-EM like reconstruction algorithm for emission tomography," *Proc. SPIE Med. Imag.*, vol. 4684, pp. 10–19, 2002.

[7] P. Khurd, I.-T. Hsiao, A. Rangarajan, and G. Gindi, "A globally convergent regularized ordered-subset algorithm for list-mode reconstruction," *IEEE Tran. Nucl. Sci.*, vol. 51, no. 6, pp. 719–725, Jun. 2004.

[8] R. Levkovitz, D. Falikman, M. Zibulevsky, A. Ben-Tal, and A. Nemirovski, "The design and implementation of COSEM, an iterative algorithm for fully 3-D listmode data," *IEEE Trans. Med. Imag.*, vol. 20, no. 7, pp. 633–642, Jul. 2001.

[9] I.-T. Hsiao, A. Rangarajan, P. Khurd, and G. Gindi, "An accelerated convergent ordered subsets algorithm for emission tomography," *Phys. Med. Biol.*, vol. 49, no. 11, pp. 2145–2156, 2004.

[10] A. Rahmim, J. C. Cheng, S. Blinder, M. L. Camborde, and V. Sossi, "Statistical list-mode image reconstruction for the high resolution research tomograph," *Phys. Med. Biol.*, vol. 49, no. 8, pp. 4239–4258, 2004.

[11] R. M. Neal and G. E. Hinton, *A View of the EM Algorithm That Justifies Incremental, Sparse, and Other Variants*. Boston, MA: Kluwer, 1998, pp. 355–368.

[12] J. Browne and A. D. Pierro, "A row-action alternative to the EM algorithm for maximizing likelihoods in emission tomography," *IEEE Trans. Med. Imag.*, vol. 15, no. 5, pp. 687–699, May 1996.

[13] R. Siddon, "Fast calculation of the exact radiological path length for a three-dimensional CT array," *Med. Phys.*, vol. 12, no. 2, pp. 252–255, 1985.

[14] H. Zhao and A. J. Reader, "A fast ray-tracing technique to calculate line integral paths in voxel arrays," in *Proc. IEEE Nuclear Science Symp.*, 2003, pp. 211–218.

[15] C. Schretter, "A fast tube of response ray-tracer," *Med. Phys.*, vol. 33, no. 12, pp. 4744–4748, 2006.

[16] P. E. Kinahan, D. W. Townsend, T. Beyer, and D. Sashin, "Attenuation correction for a combined 3D PET/CT scanner," *Med. Phys.*, vol. 25, no. 12, pp. 2046–2053, 1998.

[17] S. Ahn, J. A. Fessler, D. Blatt, and A. O. Hero, "Convergent incremental optimization transfer algorithms: Application to tomography," *IEEE Trans. Med. Imag.*, vol. 25, no. 3, pp. 283–296, Mar. 2006.

[18] T. Mitchell, *Machine Learning*. New York: McGraw Hill, 1997.

[19] W. P. Segars, "Development and Application of the New Dynamic NURBS-Based Cardiac-Torso (NCAT) Phantom," Ph.D. dissertation, Univ. North Carolina, Chapel Hill, 2001.

Colas Schretter graduated with Great Honours in computer science from the Université Libre de Bruxelles (ULB), Belgium, in 2003. He is currently pursuing the Ph.D. degree in motion estimation and compensation in computed tomography.

He is currently with Philips Research Europe, Aachen, Germany, a position funded by the Marie Curie early stage training program of the European commission. His main interests include theoretical aspects of computer science, computer programming, geometric algorithms and data structures, real-time computer graphics, bioinformatics, and image reconstruction in emission and transmission tomography.